Phys Chem Minerals (2003) 30: 631–640
DOI 10.1007/s00269-003-0352-0

ORIGINAL PAPER

A. P. Radlinski · J. Claoué-Long · A. L. Hinde
E. Z. Radlinska · J.-S. Lin

Small-angle X-ray scattering measurement of the internal microstructure of natural zircon crystals

Received: 8 October 2002 / Accepted: 1 July 2003

Abstract Zircon crystals change their physical properties significantly over time in response to the radiation damage (metamictization) induced in the lattice by the presence of radionuclides U and Th. Crystalline zircon has extremely low diffusion rates of the radiogenic daughter product, Pb. Lead diffusion is enhanced in metamict volumes, but the observed lack of correlation between Pb loss and metamictization in natural zircons requires that other mechanisms control the incidence of Pb migration. The proposition that self-induced stress and elasticity contrasts in zoned natural crystals create fast-track Pb migration pathways, in response to time-integrated radiation damage, requires a means of detecting the microstructures within zircons at the interatomic scale at which Pb migration takes place. Small-angle X-ray scattering (SAXS) is introduced as a means of detecting candidate microstructures including subgrain boundaries, defect networks and microfractures produced by differential metamictization. It is shown that a classical X-ray source yields measurable SAXS response from contrasting metamict and crystalline domains within a crystal, and these properties are quantified for a metamict zircon megacryst. Detection of the weaker SAXS response expected from microfractures and networked defects requires the more intense X-rays of synchrotron-source radiation.

A. P. Radlinski · J. Claoué-Long (✉) · A. L. Hinde
Geoscience Australia, GPO Box 378,
Canberra, ACT 2601, Australia
e-mail: Jon.Long@ga.gov.au
Fax: +61 (0)2 62499971; Tel.: +61 (0)2 62499418

E. Z. Radlinska
Department of Applied Mathematics,
Australian National University,
Canberra ACT 0200, Australia

J.-S. Lin
Condensed Matter Sciences Division,
Oak Ridge National Laboratory,
Oak Ridge, Tennessee 37831-6377, USA

Introduction

In the search for mechanisms that explain why zircon U–Pb isotopic dating of geological systems works so well, or alternatively fails to work well in some circumstances, the most interesting idea to emerge in the past decade has been the multipath diffusion proposal of J.K.W. Lee and coworkers. A series of contributions (Lee 1993, 1995; Lee and Tromp 1995) developed the notion that simple volume diffusion within a crystal medium may not be the dominant, or at least not the only, mechanism by which radiogenic isotopes can migrate from a phase whose retention of those isotopes is vital to recording a geological age. Instead, other, faster pathways to diffusion may develop in response to the complex zoning of natural crystal compositions, and complex histories of metamictization, annealing and recrystallization. Isotopes within a crystal that escape from the crystalline volume into within-grain shortcuts may bypass volume diffusion as the dominant process and migrate rapidly by grain boundary or fluid-enhanced transport processes. The multipath diffusion proposal is controversial in its application to, for example, feldspar Ar/Ar isotopic because the alternative mechanism of volume Ar diffusion within crystals may also provide satisfying explanations of the majority of measured Ar retention behaviours and isotopic compositions (McDougall and Harrison 1999). In the field of zircon U–Pb dating, explanations of the degree and incidence of Pb isotopic leakage in crystals are much more problematic (see below), and little progress has been made for a reason originally identified by Lee (1993, p 440): the lack of techniques with which to detect the real diffusion pathways in geological samples at the interatomic scale at which Pb migration takes place. The multipath diffusion model as a candidate explanation has thus remained a good, but untestable, idea.

The problem of understanding microscale mechanisms of Pb retention and migration in zircon is acquiring urgency with the advent of routine microbeam

U–Pb dating by SHRIMP ion microprobe (Compston et al. 1984). The 10–30-μm spatial resolution of SHRIMP analysis reveals complex variations in Pb retention within single zircon crystals (Williams 1998), and these require a satisfying explanation that relates measured compositions to the nature and history of the sample (e.g. Nasdala et al. 1998). SHRIMP measurement depends heavily on the use of natural zircons as laboratory reference materials so it is vital also to benchmark the microstructural and isotopic integrity of zircon reference materials at high spatial resolution, to underpin the reliability of laboratory procedures based on their compositions.

This contribution introduces the technique of small-angle X-ray scattering (SAXS) as a direct and non-destructive means of both detecting and measuring the microstructure of natural zircon crystals at the interatomic scale that governs Pb migration. The SAXS technique, first developed about 70 years ago, has been widely used for microstructural studies in physics, chemistry, materials sciences, colloids and polymer science, metallurgy, biology and other fields. SAXS is a non-invasive technique that provides quantitative insight into the microstructure of regions with electronic density contrast, volume-averaged over the entire sample irradiated with the incident X-ray beam (Guinier et al. 1955; Glatter and Kratky 1982; Lindner and Zemb 1991), in a way similar to that by which the classical X-ray diffraction (XRD) technique provides quantitative information about the crystalline lattice geometry, averaged over the sample volume. Both SAXS and XRD respond to small-scale fluctuations of the electronic density within the scattering medium. The difference between XRD and SAXS is that XRD is sensitive to the interatomic distances roughly within the range 0.5 to 10 Å, whereas SAXS provides information about the electronic density fluctuations in the linear size range 10 to about 3000 Å.

In geosciences, the SAXS technique has previously been applied to detecting the microstructural hydrocarbon migration pathways within petroleum source rocks, and the porosities controlling methane migration within coals (Radlinski et al. 2000, 2001). The microstructure of zircon at the interatomic scale that governs Pb migration is an analagous problem. In this introductory work we document the method and demonstrate that SAXS can non-invasively detect and document atomic-scale microgeometries previously imaged in well-studied natural zircon megacrysts by invasive transmission electron microscopy (TEM). As the interpretation of SAXS data is based on specific microstructural models, these are, in turn, tested against the direct imaging methods, TEM in this case. It is important to note that whereas TEM generates a direct microstructural image for a laboriously prepared small (and not necessarily representative) local sample of the macroscopic material (zircon crystal in this case), SAXS produces non-invasively an average over the entire sample volume sampled by the X-rays, with the structural information in the form of the volume average of the density–density correlation function. The SAXS and TEM techniques are, therefore, complementary; the microstructural models derived from SAXS can be tested by TEM imagery and, conversely, the SAXS scattering curves can be constructed numerically from statistical averages of a large number of local TEM images (Radlinski et al. 2003).

The SAXS experiments reported in this work were performed using a SAXS instrument equipped with a classical X-ray source producing a broad 2-mm diameter beam, which averages the microstructural information over a large volume of the entire zircon. The success of this work has paved the way for detailed mapping of a richer range of zircon microstructures in natural zircon crystals using a microbeam SAXS technique, which employs a synchrotron-generated X-ray beam focused to a microbeam at the same 20-μm probe scale that the SHRIMP uses for measuring U–Pb isotopic compositions; this expansion of the investigation will be reported elsewhere.

Microstructural possibilities in natural zircons

Natural zircon crystals ($ZrSiO_4$) containing trace quantities of uranium and thorium are widely used for measuring the ages of rocks. Radionuclides ^{238}U, ^{235}U and ^{232}Th and their daughter products transform through a series of decay events into ^{206}Pb, ^{207}Pb and ^{208}Pb, respectively. With knowledge of the half-lives for each of these decay schemes, the accumulation of daughter isotopes becomes a measure of the time elapsed since the zircon crystal became closed to U–Th–Pb isotopic diffusion (Faure 1986).

When we seek to interpret geological age information from the Pb accumulation clock(s), there are two separate problems innate to the nature of the zircon crystal itself. One is the capacity of zircon crystals to record more than one isotopic age by retaining inherited isotopic compositions through overprinting processes and events, including partial recrystallization and overgrowth of new crystallization, owing to the extremely slow rate of diffusion of U and Pb within the zircon medium under a wide range of geological conditions. This problem has largely been solved and turned into a benefit by the advent of SHRIMP microbeam analysis which can probe the isotopic zoning within individual crystals and, in favourable circumstances, unravel complex multievent geological histories (Williams 1998).

An opposing problem is the failure of some zircon crystals to retain their original U–Pb isotopic compositions and ages, in certain circumstances. Clearly this must reflect short circuit diffusion and leakage of Pb isotopes from some zircon crystals, but candidate Pb loss mechanisms remain poorly understood and it is rarely evident why some zircon crystals retain isotopic integrity while others — even in the same rock — do not.

The rate of volume diffusion of Pb in crystalline zircon is so extremely slow that loss of significant amounts

of Pb by volume diffusion is inconceivable at geologically reasonable temperatures. Cherniak and Watson (2000) demonstrate that a near-perfect, defect-free crystalline zircon of 10 μm radius would lose only about 1% of its Pb by diffusion if residing at 750 °C for times of the order of the age of the Earth. Most zircons used in geochronology have a diffusion radius much larger than 10 μm and will therefore retain Pb isotopes over geological times if they are in the crystalline state.

Natural zircon is rarely in a perfect crystalline condition, however, owing to the self-induced radiation damage it experiences from the decay of U and Th, and their unstable daughter nuclei, over time. Here lies the likely explanation for the otherwise puzzling discrepancy in Pb diffusion rates reported from separate experiments on natural zircon by Lee et al. (1977) and Cherniak and Watson (2000). The latter used perfect synthetic zircons and a natural zircon so anomalously low in U and Th content as to approach radiation-free crystalline condition. Lee et al. (1997) used a natural zircon with a higher (and geologically more typical) content of U and Th and therefore some internal radiation damage. The faster diffusion rate measured in the latter material infers the potential that crystal defects strongly influence zircon Pb diffusion behaviour.

When radiation-induced lattice damage becomes advanced, crystalline zircon is reduced to an amorphous condition known as the metamict state (Holland and Gottfried 1955). Pb loss from metamict zircons is more likely since diffusion rates have been found to be much more rapid in radiation-damaged crystals (Cherniak et al. 1991). Metamictization is a response to the radiation dose, itself a function of U and Th content and the time elapsed since a crystal formed. If radiation dose were the only factor controlling metamictization, then most zircons with moderate or higher uranium contents and more than 1–2 Ga old should have become metamict and lost significant proportions of Pb by accelerated volume diffusion within the amorphous phase (Cherniak and Watson 2000). This does not accord with observations of natural zircons, many of which have retained Pb isotopes over even longer periods of time (e.g. Froude et al. 1983). In the zircons sampled from an individual rock, a degree of correlation between U content and Pb loss is sometimes found, indicating a role for the enhanced diffusion in the more radiation-damaged zircons; but more often there is a lack of any obvious correlation between Pb loss and the radiation dose a crystal has experienced (e.g. Pigeon et al. 1998).

Part of the reason for the discrepancy is that the degree of amorphization in any crystal will be a complex function of its time–temperature history as well as its radiation dose, because at elevated temperatures an opposing process of natural annealing of radiation damage takes place on geological time scales. Even zircons with moderate to high uranium contents, if held above a "critical amorphization temperature" in the range of greenschist facies metamorphic temperatures (about 350 °C), may not become metamict at all (Cherniak and Watson 2000). Thus metamictization in zircon is a function of the degree to which radiation damage has been permitted to accumulate, not simply a function of the radiation dose, and this will be controlled by the individual crustal (i.e. thermal) histories of the rocks and zircon crystals being studied. Taken further, should the thermal history include sequential periods of metamictization, annealing and/or recrystallization, then Pb loss may not be controlled by volume diffusion at all but by decomposition processes and the movement of reaction fronts which can be connected with extensive migration of elements. As any accumulated Pb is incompatible in a recrystallizing lattice, it may be more or less completely excluded, leading to partial or complete resetting of the Pb accumulation clock locally within a crystal (McLaren et al. 1994).

The temperature–time history since a crystal initially formed, leading to the degree of metamictization, annealing and recrystallization, is a reflection of the environment external to the crystal. If these factors alone controlled the degree of Pb mobility in a crystal, then the degree of retention of Pb by zircon crystals would provide a recorder of the geological event histories they have experienced. A simple test of this would be to establish whether Pb loss in natural zircons is correlated with the degree of accumulated metamictization, as distinct from the radiation dose experienced. This experiment has been done. Raman spectroscopy — specifically, shifts and broadening of peaks in the Raman spectrum — has proved to be a good measure of the accumulated metamictization in a zircon lattice and can be applied within crystals at volume scales of observation down to a few μm. Nasdala et al. (1998), in a detailed Raman study of metamictization and Pb loss in natural zircons from a range of geological situations, did find a degree of correlation between measured metamictization and Pb loss, but, significantly, found the correlation to be highly variable and unpredictable. This has led to the critically important observation that metamictization alone is not the primary cause of accelerated Pb loss in natural zircons. Metamictization only enhances the probability of Pb loss: other, unidentified, factors control whether or not it actually occurs.

The answer to this apparent conundrum almost certainly lies in the observation, also from detailed Raman spectroscopy, that natural zircons are heterogeneously metamict (Nasdala et al. 1996). This is a consequence of the zoned distribution of radionuclides and other trace elements substituted in the zircon lattice and the extremely local radiation damage the radionuclides cause. A wide variety of trace-element zoning patterns are encountered at width scales anywhere between one to a few hundred micrometres, an especially common variant being oscillatory concentric growth zones, with abrupt boundaries separating order-of-magnitude differences in radionuclide content (Chakoumakos et al. 1987). The striking feature of Raman studies correlated with element concentration measurements in zoned zircons is

that the boundaries between high and low radionuclide zones are identical to the boundaries between high and low metamictization. The sharpness of the structural change matches the sharpness of the chemical boundary down to the scale limit of Raman probe observation of approximately 1 μm (Nasdala et al. 1996). If the dominant causes of radiation damage in zircon were the tracks of alpha radiation from uranium decay, then diffuse haloes of damage with a width up to 10–30 μm should penetrate from high- into low-radionuclide zones (Ewing et al. 1987). The fact that this is not observed requires that the alpha recoil process — recoil of the U or Th nucleus after emitting a He^{2+} ion — is the dominant cause of lattice damage and amorphization. Recoil has a length scale in the range of 30–35 nm (Yada et al. 1987). The critical consequence of this observation is that extremely high gradients of structural change are developed and maintained at within-crystal chemical boundaries such as growth zones. Among the physical effects of amorphisation in the high-radionuclide zones of zircon are a decrease in the elastic moduli of up to 69% (Ozkan 1976); and volume expansion of up to 6% of the unit cell while it remains in a crystalline state (Salje et al. 1999), with up to 18.4% volume expansion when production and progressive accumulation of amorphous metamict regions responds to an accumulated radiation dose in excess of about 3×10^{15} α decays mg^{-1} (Weber 1993). Differential expansion of the zones within a crystal will inevitably lead to large internal stress and elasticity contrasts focused at the zone boundaries (Lee and Tromp 1995). These will generate significant microstructural change and potential ways in which Pb isotope diffusion within the volume of zircon could be bypassed or accelerated, including (1) reduction of the crystal volume into a large number of smaller subdomains, reducing the effective diffusion radius that a Pb isotope must traverse to escape, and (2) development of microfracture or crystal defect pathways which, should they become networked, offer potential for fast grain-boundary or fluid-enhanced migration (Lee 1993). Should these or other microstructural responses occur, then it may be postulated that volume diffusion, within either the crystalline or metamict zircon state, will not be the dominant process that governs Pb loss from zircon. Instead, the governing mechanism will be the geometry and networking of microstructural failure within crystals at the interatomic scale and provision of fast-track pathways. In turn, this will be a complex response to the individual radionuclide zoning patterns (and therefore heterogeneous metamictization) individual to each crystal.

The final point to bear in mind is that the development of internal microstructures in zircons will be a time-integrated evolution from which today we observe only the end result. A zircon observed to be pervasively metamict today will have passed through earlier stages of heterogeneous internal stresses during which it may have developed microstructures that have since been obliterated by continued radiation damage, volume expansion and change in elasticity. Alternatively, a zircon may be observed to be highly fractured today because it has released stress by fracturing upon exhumation from crustal depths to the surface, so its current structural state could belie the fact that it spent most of its history buried at depths where self-annealing precluded the development of heterogeneous metamictization. The main control will be the temperature–time history of the crystal. Lee and Tromp (1995) calculated that sustained confining pressures under deep burial will also inhibit formation of internal fractures, but the confining pressures needed correspond to crustal depths of 30–40 km, at which the ambient granulite facies metamorphic temperatures will be a far greater influence on the process of self-annealing than the pressure.

A macro approach to the development of the internal microfractures of zircon was initiated by Lee and Tromp (1995), who modelled the development of alternate concentric or radial fractures in zircon crystals from fracture mechanics theory and found that large visible cracks in simply zoned natural zircons match the predicted stress patterns in both their location and geometric orientations. Pb migration occurs at interatomic scales well below that of visible cracking, so their observations do not apply to the Pb migration problem directly unless the pathway developments are scale-invariant (i.e. fractal), such that the visible scale of observation is an analogue of microstructures at the interatomic scale. Raman spectroscopy has proved a useful tool for examining the crystalline state of the lattice at spatial scales down to the 1–3 μm-diameter of the available laser-probes, but this technique images only the phonon vibrations from the lattice and so cannot produce information about the whole range of potential interatomic migration pathways such as defect networks, subgrain boundaries within crystals and microfractures. SAXS overcomes this limitation by detecting and quantifying the wider range of zircon microstructures that scatter X-rays, directly at the relevant interatomic scale.

The samples

Our purpose in this preliminary contribution is to introduce the SAXS technique in zircon by an application to two relatively simple zircon megacrysts. These large crystals are not perfectly homogeneous in the distribution of radionuclide contents, and hence radiation damage – no natural zircon crystal offers this ideal — but the measured internal variations in their radionuclide contents are relatively low, of the order of ±20% (Compston et al. 1984; Claoue-Long et al. 1995). Thus, they lack juxtapositions of the order-of-magnitude contrasts which can lead to differential metamictization, sharp local contrasts in volume expansion and responses such as microfracturing. As such, they are suitable for demonstrating the detection of microstructures in relatively simple situations. The range of complex

microstructures developed in a range of more typical, heterogeneous and zoned zircons have since been studied using microbeam synchrotron SAXS and will be reported elsewhere.

The SL13 and SL3 zircon megacrysts both derive from the gem gravels in Sri Lanka and they have been used in the past as laboratory standards for ion microprobe analysis of U–Th–Pb isotopic compositions and ages. Their crystallization ages are similar, between 550 and 585 Ma (Compston et al. 1984; Claoue-Long et al. 1995). SL3 has a high U content of approximately 3500 ppm and has experienced a high time-integrated radiation dose; it has been the subject of earlier microstructural study using TEM imaging (McLaren et al. 1994). SL13 has a relatively low U content of approximately 240 ppm and consequently has experienced an order-of-magnitude lower radiation dose over the same period of time. Murakami et al. (1991) analyzed the effect of radiation damage on the density, X-ray diffraction patterns and high resolution TEM for about 200 crystals of zircon from the same Sri Lankan gem locality, containing from several tens to several thousands ppm of uranium and thorium, corresponding to the dose 0.06×10^{15} to 6.8×10^{15} alpha decays mg^{-1}. It transpired that a transition to the metamict (amorphous) state occurs in these megacrysts in the dose range 1×10^{15} to 8×10^{15} decays mg^{-1}, corresponding to the uranium concentration range 500 to 3000 ppm. It has since been shown that these are underestimates of the rate of metamictization because the Sri Lankan zircon megacrysts have accumulated less radiation damage than is indicated by their time-integrated dose (Nasdala et al. 2001), meaning that the crystals have resided in the temperature range of at least partial self-annealing for a significant part of their history. On this basis, SL13 is predicted to remain predominantly crystalline (only slightly radiation-damaged) today, and SL3 should be in a pervasively metamict state. Both crystals have been broken into small random fragments for repeated isotopic analysis and shards of unknown crystal orientation approximately 1–2 mm across were selected for the SAXS work.

The method

SAXS measurements were performed using the 10-m SAXS facility at the Oak Ridge National Laboratory (Russell et al. 1988). The resolution of this instrument allows coverage of the linear size range of the scattering objects from 1 nm (10 Å) to 25 nm (250 Å). The instrument is equipped with a rotating anode Cu K_α X-ray source $\lambda = 1.54$ Å). The X-ray beam diameter at the sample is about 2 mm, and lead apertures were used to ascertain that there was no leakage of X-ray photons around the natural zircons samples. Since the Cu K_α linear absorption coefficient for crystalline zircon is high (397 cm^{-1}), in order to maintain a reasonable X-ray transmission it was necessary to prepare sections of crystals about 10 μm thick. Properties of SL3 and SL13 crystals used for SAXS work are listed in Table 1.

Reference has been made above to the utility of Raman imaging to provide measurements of the degree of degradation of the lattice (metamictization) accumulated in a zircon crystal, at spatial scales of observation down to approximately 1 μm. It has also been postulated above that such metamictization is not the major control on Pb migration in zircon, but instead there is dependence on the idiosyncratic microstructures developed in response to differential metamictization and volume expansion stresses within individual crystals. Thus there is a need for a method of detecting microstructures that Raman cannot detect, such as intra-grain boundaries, microfractures of various orientations, networked defects, networked amorphous zones etc. at the interatomic scale at which migration of Pb isotopes takes place. SAXS is well suited to this purpose. Information pertinent to the concentration and size distribution of scattering objects in a volume (boundaries of intracrystalline regions in the simple case of the megacrysts studied here) can be retrieved from the absolute scattering intensity (measured as the number of X-ray photons scattered from the incident beam of known intensity, within the differential solid angle $d\Omega$ with sample at its apex, and per unit sample volume). The scattering intensity is measured versus the scattering vector, $\mathbf{Q}$:$\mathbf{Q} = (4\pi/\lambda) \sin(\Theta/2)$ where Θ is the (small) scattering angle defining the scattering differential solid angle $d\Omega$ and λ is the wavelength of X-rays (Guinier et al. 1955; Espinat 1990; Lindner and Zemb 1991). As Θ is measured from the direction of the incident beam and, for typical SAXS experiments, does not exceed 5°, SAXS experiments measure the scattering intensity looking through the sample almost directly into the X-ray source, and the scattering vector, $\mathbf{Q}$, is practically proportional to the scattering angle, Θ, and expressed in units of $Å^{-1}$ rather than degrees.

SAXS can be applied to detect and quantify scattering objects of any geometry. In the unlikely situation where the individual geometry of every single scattering object within a zircon volume is known, then the scattering intensity versus $\mathbf{Q}$ can be calculated exactly from the geometrical information and the scattering contrast, which reflects the difference between the electronic density of the scattering object and the matrix within which it is embedded. In general, the contrast is defined by differences between the elemental compositions (hence the number of electrons) and specific densities (hence the volume within which the electrons are confined) of these two regions. For zircons, the scattering occurs between the crystalline and amorphous regions and the contrast occurs exclusively because of the differences in specific density between those two regions.

Here, we have the more usual inverse situation of measurements of scattering intensity versus $\mathbf{Q}$ over a range of $\mathbf{Q}$, and must gauge the theoretical fit of the scatterer size distribution to expectations about the geometry and size distribution of the scattering objects within the crystal. In the simple situations tested here the target expectation is of polydisperse spheres, and we have the further quantification of knowing the scattering contrast between metamict and crystalline zircon (see Appendix). The shape

Table 1 Properties of zircon crystals used in SAXS experiments. Note that uranium concentrations are averages of the measurements for multiple fragments of each crystal

Crystal	Origin	Approximate age	Uranium concentration (ppm)	Thickness (μm)	Surface area (mm^2)	X-ray transmission
SL3	Sri Lanka megacryst	550–580 Ma	3500	11 (±1)	3.87	0.58
SL13	Sri Lanka megacryst	550–580 Ma	240	10 (±1)	0.97	0.89

expectation arises because there have been very many independent radioactive decays within the X-rayed volumes, so the radiation damage should be distributed pervasively throughout the volume. The independence of each individual decay means that there is no correlation between various damaged regions or regularity in the pattern of damage. Finally, the damage is directionally isotropic, leading to the sphere as the model shape of locally damaged regions. TEM images of the heavily metamict SL3 crystal (McLaren et al. 1994) do show two-dimensional cross-sections of coalesced amorphous regions which are approximately circular, which corroborates the quantitative structural model based on SAXS data. The X-ray scattering response will be similar for other shapes whose three dimensions are approximately the same (such as cubes or fat discs), but will be very different if the scattering objects include flat shapes (two-dimensional) or needles (one-dimensional).

As discussed below, the SAXS contrast in these zircons originates from the density difference between the amorphous regions and remaining crystalline volumes. Amorphization in natural zircons containing uranium and thorium is potentially caused by two types of events. There is the creation of several hundreds of Frenkel defects towards the end of the 10–30-μm-long ionization track of the 4.5–5.0 MeV α particles, and there is the synchronous formation of very short, but much more intensely damaging, amorphous tracks approximately 10 nm long (several thousand atomic displacements) by α-recoil atoms with energy range from 0.07 MeV (^{232}Th decay) to 0.17 MeV (last decay in the ^{232}Th series, ^{212}Po decay) (Murakami et al. 1991). At sufficiently high radiation doses the individual damaged tracks coalesce and a continuous amorphous phase is formed. The geometry of remaining crystalline "islands" can reasonably be represented as polydisperse, roughly spherical regions.

The dominant contribution to the scattering intensity, measured at a particular value of **Q**, comes from scattering regions within the linear size range $2.5/\mathbf{Q} \pm 50\%$ (Radlinski et al. 2000). Therefore, the experimental **Q** range used in this work, $0.01\ \text{Å}^{-1} < \mathbf{Q} < 0.3\ \text{Å}^{-1}$, corresponds to the linear size range $0.8\ \text{nm} < r < 25\ \text{nm}$. Judging from TEM images (McLaren et al. 1994), this range is sufficient to cover the sizes of crystalline regions present in SL3.

Below we demonstrate that the geometry of scattering regions in SL3 can be reasonably approximated as a collection of spheres with a wide distribution of diameters. The absolute scattering intensity for an arbitrary distribution of spheres can be derived assuming a distribution, $f(r)$, for the radii (Radlinski et al. 2001):

$$I(\mathbf{Q}) = (\rho_1 - \rho_2)^2 \frac{\phi}{\bar{V}_r} \int_{R_{\min}}^{R_{\max}} V_r^2 f(r) F_{\text{sph}}(\mathbf{Q}r) dr \ , \quad (1)$$

where ρ_1 and ρ_2 is the scattering length density for the scatterers and the matrix, respectively, Φ is the volume fraction occupied by the scatterers (regions of amorphous phase in this case), $R_{\min}$ and $R_{\max}$ are the minimum and maximum scatterer radii in the distribution $f(r)$, respectively, **Q** is the scattering vector, r is the scatterer radius, F_{sph} is the scattering form factor for a sphere, $V_r = (4/3)\pi r^3$ is the scatterer volume and $\bar{V}_r = \int_0^\infty f(r)dr$ is the average scatterer volume.

Furthermore, for numerical convenience, the size distribution may be expressed as a histogram:

$$I(\mathbf{Q}) = \sum_i I\mathbf{Q}_{0i} \frac{\int_{R_{\min}}^{R_{\max}} V_\Gamma^2 F_{\text{sph}}(\mathbf{Q}r)\, dr}{(R_{\max_i} - R_{\min_i})} \ , \quad (2)$$

where $I\mathbf{Q}_{0i} = \frac{(\rho_1 - \rho_2)^2 \phi}{\bar{V}_r} f(r_i)(R_{\max_i} - R_{\min_i})$, and the summation is over the histogram cells. The other quantities are the scattering contrast:

$$\overline{\Delta\rho^2} = (\rho_1 - \rho_2)^2 \phi(1 - \phi) \quad (3)$$

and the scattering form factor for a sphere of radius r:

$$F_{\text{sph}}(\mathbf{Q}r) = \left[3 \frac{\sin(\mathbf{Q}r) - \mathbf{Q}r \cos(\mathbf{Q}r)}{(\mathbf{Q}r)^3} \right]^2 . \quad (4)$$

For radiation-damaged zircons, the scattering of X-rays takes place at the interface between the crystalline and amorphous region. The quantities ρ_1 and ρ_2 are the scattering length densities of the two phases. The scattering length density for X-rays is given by:

$$\rho = (N_A d/M) N_e I_e \ , \quad (5)$$

where N_A is Avogadro's number, d is density, M is the molar mass and $I_e = (e^2 mc^{-2})$ is the scattering amplitude for a single electron. N_e is the number of electrons in one "supramolecule" of composition corresponding to the average elemental composition of a macroscopic phase present in the scattering medium (crystalline zircon or metamict zircon in this particular case), $\Sigma_j p_j (\Sigma_i s_i)_j$, where s_i is the proportion by number of atom i in the compound j and p_j is the proportion by molecular number of compound j in the macroscopic phase. For unaltered zircon, $ZrSiO_4$, there is only one compound in the scattering medium, corresponding to $j = 1$, but the scattering length density for the crystalline phase is different to that of metamict phase owing to different density. The number of phases can increase in thermally annealed zircons, where phase transitions and precipitates of SiO_2 have been observed (McLaren et al. 1994). Table 2 lists calculated scattering length densities for crystalline and amorphous zircons.

Shards of the two Sri Lankan zircon megacrysts were prepared as doubly polished wafers approximately 10 μm thick so as to present a parallel-sided volume thin enough to permit adequate transmission through zircon from a classical Cu Kα X-ray source and return X-ray scattering information. The experiment was conducted in vacuum to reduce the scattering background from air, but there is a significant background correction for the scattering response of a nylon mesh to which the fragile zircon wafers were attached. The 2-mm diameter X-ray beam employed in this study has acquired an aggregate SAXS signal from the entire volume of the megacryst wafers presented to it.

SAXS results

The most important result of the experiment is the first-order difference in SAXS response between the two crystals. There is no detectable SAXS signal from the 1-mm^2 area by 10-μm-thick volume of SL13, apart from a small artefact resulting from subtracting background scattering from the support mesh, indicating

Table 2 Properties of amorphous and crystalline zircons pertinent to SAXS data interpretation. Values of density are taken from Murakami et al. (1991). Note that a range of values as low as 3.86 is possible for the density of more extremely metamict zircon. For details of calculations see Appendix

Crystal type	Density d (g cm^{-3})	Molar mass M (g)	Number of electrons N_e	Scattering length density ρ ($\times 10^{11}$ cm^{-2})
Fully crystalline $ZrSiO_4$	4.72	183.3	86	3.76
Fully amorphous $ZrSiO_4$	4.0	183.3	86	3.18

that this low-uranium megacryst remains in a uniform crystalline state devoid of significant internal microstructure. This outcome supports the measurements of Murakami et al. (1991), which indicated that zircons in the Sri Lankan megacryst suite with uranium contents below about 500 ppm U remain crystalline. If there exist microstructures within SL13 they will not be associated with a volume fraction of metamict phase above the SAXS-detectable threshold which, assuming a size distribution similar to that presented in Fig. 3, we estimate to be about 0.5%. Instead, the dominantly crystalline sample is likely to contain atomic-scale defect networks, or microfractures developed from brittle fracture of the crystal. SAXS should detect such a network, if present at large enough concentration, because a scattering signal will be returned from the interface between the crystalline phase and the void in the defect network or microfracture. However, the strength of the scattering signal in the large-**Q** limit is proportional to the surface area of the network and will be very much weaker than the SAXS return from gross volume boundaries. The significant scattering background correction in this particular experiment makes it possible that detection of microfracture networks is hidden in a low signal/background ratio. The solution to this limitation is use of a more sophisticated sample-mounting technique.

In contrast to SL13, a strong scattering is observed from SL3 (Fig. 1). This is expected since SL3 contains an order of magnitude more uranium than SL13 and should have accumulated significant radiation damage. TEM imaging of a different fragment from SL3 has shown that this megacryst is composed dominantly of regions of amorphous phase in which are embedded remnant crystalline domains, with the linear sizes of single crystalline domains in the range 20 to 150 Å (in Fig. 5 McLaren et al. 1994).

A fit of SAXS data to the model of polydisperse spheres (Eq. (2)) is shown in Fig. 2 with a solid line. The maximum scattering intensity is about 3×10^3 cm^{-1} and the scattering background is 0.4 cm^{-1}. A flat scattering background of this magnitude is characteristic of various geological materials and indicates the presence of small-scale (less than 10 Å across) electron density inhomogeneities (microstructural and/or compositional) within the crystal. In the large-Q limit the scattering intensity decreases according to a power law with the exponent –4.2, which in the log-log representation gives a straight line with slope equal to –4.2. Given the quality of our data, this is significantly less than the classical Porod limit exponent of –4.0 (Guinier et al. 1955) expected and frequently observed in SAXS data for perfectly smooth phase boundaries, which is the SAXS signature of certain roughness on the scale of 50 Å and less within the transition zone of the amorphous-crystalline interface (cf. McLaren et al. 1994).

The distribution of the scattering domain size, expressed as a histogram and calculated according to Eq. (2) by fit to experimental SAXS data, is illustrated in Fig. 3. The distribution is exponential within experimental error, meaning that there is an exponentially increasing quantity of progressively smaller domains down to the size limit of detection. The limiting linear domain sizes obtained from the best fit are $R_{\min} = 28$ Å

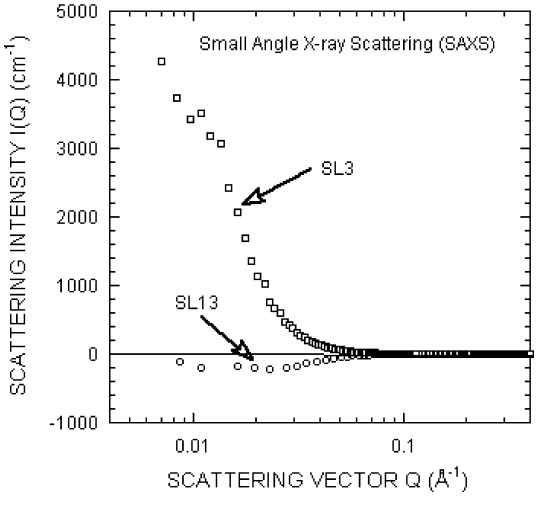

Fig. 1 Absolutely calibrated raw SAXS data for zircons SL3 and SL13. There is no detectable scattering signal from SL13. Negative values in the small-**Q** range are an artefact due to the processing of a weak noisy signal with a relatively high background correction. The *curve* for SL13 demonstrates that the presence of the support mesh scattering signal can distort the scattering curve by up to 200 cm^{-1} for $\mathbf{Q} < 0.05$ Å^{-1}. The SAXS machine used in this work has the scattering intensity absolutely calibrated within ± 10%, and the SAXS data acquisition time has been selected to introduce no more than 5% statistical error for every data point shown

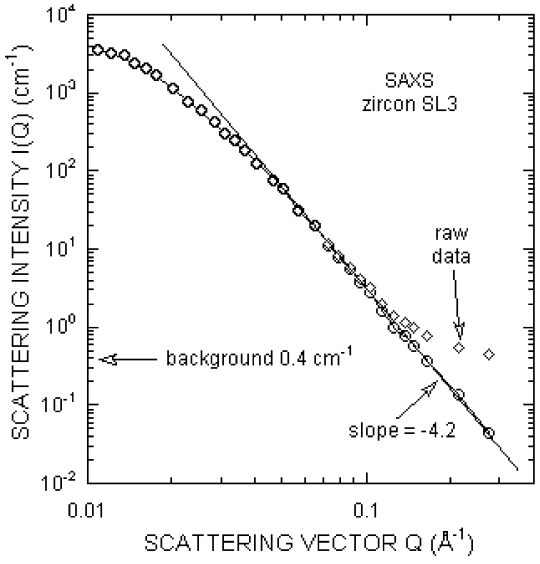

Fig. 2 Analysis of SAXS data for zircon SL3. *Diamonds* Absolutely calibrated raw data; *open circles* raw data with subtracted background scattering; *solid line* fit to the model of scattering by polydisperse spherical domains. The slope of –4.2 in the large-**Q** region indicates a rough, but non-fractal interface between the crystalline and metamict regions

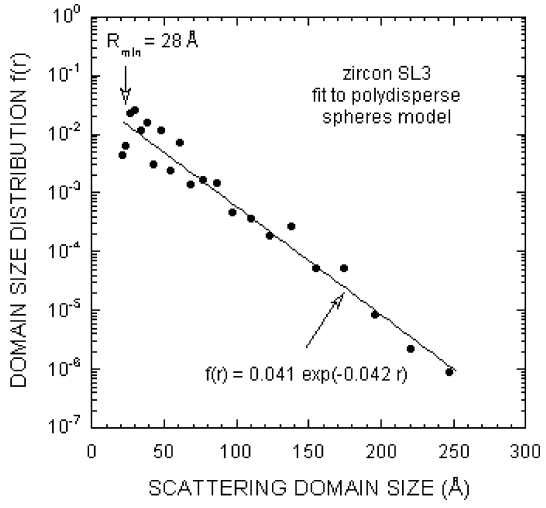

Fig. 3 The distribution of scattering domain sizes obtained from the fit to the polydisperse distribution (Fig. 2). The linear size of the domain, *r*, appears to be distributed according to an exponential law over at least one order of magnitude. The minimum domain size is 2.8 nm, whereas the maximum domain size can be larger than the experimentally limited value of about 30 nm

and $R_{max} = 160$ Å, in good agreement with the TEM data. The presence of a relatively very small number of domains larger than R_{max} (as shown in Fig. 3 for domain sizes up to 250 Å) does not greatly affect the quality of the fit and, therefore, is not inconsistent with current SAXS data, but would require extension of measurements into the small-**Q** domain to be properly quantified. The volume fraction ϕ of the scattering phase, calculated as the ratio of the sum of volumes of the individual scattering domains to the total sample volume, is 0.15 ± 0.05. This number could be even smaller if the density of the metamict phase were smaller than 4.0 g cm^{-3}. For instance, Nasdala et al. (2002) describe a highly metamict gem-zircon with a density of 3.86 g cm^3, which would result in the SAXS-derived volume fraction of $0.14 \pm 0.05\%$. The error is large since the volume fraction derived from SAXS data depends strongly on the number of very small scattering regions, which is not determined accurately in this experiment owing to the significant contribution of scattering background to the overall intensity in the large-**Q** region.

It is the fundamental property of small angle scattering that the shape and absolute intensity of the hypothetical SAXS curve for volume fraction ϕ of phase A embedded in the volume fraction (1-ϕ of phase B would be exactly the same as for the volume fraction ϕ of phase B embedded in the volume fraction (1-ϕ) of phase A. Therefore, it is not possible to identify the minority phase (corresponding to the volume fraction ϕ) from SAXS data alone. Direct observations by TEM (McLaren et al. 1994) as well as the results of birefringence measurements on SL3 indicate that the minority phase is the crystalline one. The volume fraction of the crystalline phase estimated from birefringence data is about 0.1, in good agreement with the SAXS-derived value of 0.15 ± 0.05.

Discussion

The theoretical approach to SAXS data obtained from natural zircons has been derived. It has been demonstrated that a still-crystalline zircon megacryst yields no detectable SAXS response, indicating a lack of internal microstructures within the crystal volume, or alternatively that the scattering response from the crystal is so weak as to be undetectable with a low-transmission X-ray source. The heavily radiation-damaged zircon SL3 returns a significant SAXS response which can be quantified as an exponential distribution of polydisperse, roughly spherical crystalline regions embedded in the amorphous matrix, the radii of the crystallites being in the range 28 to 160 Å. Such a micro-architecture of SL3 zircon indicates that (1) no atom in the crystalline lattice is more than 80 Å away from the amorphous region and (2) there is a rough crystalline–amorphous interface. We also determined the volume fraction of the crystalline phase for crystal SL3 and found it to be in agreement with earlier TEM data obtained for a single surface of the same megacryst. This provides a microstructural framework for very short diffusion paths for Pb isotopes migrating from the remaining crystalline zircon into the amorphous phase, and Pb migration within the megacryst that will be dominated by the relatively fast volume diffusion within amorphous zircon. Importantly, the remaining crystalline regions are dispersed islands whereas the dominant metamict region is continuously networked because its volume fraction is well above the percolation threshold, permitting unconstrained diffusion within that volume. We also note that no scattering objects other than the crystalline–amorphous boundaries were detected within either crystal. Although the significance of this absence is qualified by the detection limits of a classical X-ray source SAXS machine, this is in accordance with the lack of abrupt order-of-magnitude radionuclide zoning within the megacrysts, such that volume expansion and elasticity change has been relatively pervasive and uniform throughout the volume: juxtaposition of differential metamictization and resulting stress contrasts have not been important contributions towards the detectable internal microstructuring.

These results on relatively simple large zircons are in accord with previous studies of the Sri Lankan megacrysts. They serve to introduce the theory and application of SAXS to zircon structures, and demonstrate the ability of SAXS to provide quantitative insight into the volume-integrated microstructural detail in natural zircons by returning information about physical boundaries within the crystal. The information about boundaries within a volume of crystal is distinct from both TEM imaging (which returns information about a single surface) and Raman spectral analysis (which

provides data about the crystalline state within small probed volumes). The zircon volumes studied here are large because the SAXS signal was generated using a well-established and absolutely calibrated classical SAXS instrument with beam diameter about 2 mm, limiting its utility to unusually large megacrysts. With the advent of synchrotron-based microfocus SAXS technology with a beam diameter of the order of 20 μm (Riekel et al. 1998), it is now possible to X-ray the microgeometry of natural zircons of the 100–300 μm sizes typically used in U–Pb geochronology, with the same probe resolution as that of the ca. 20-μm ion beam used by SHRIMP to analyze U-Th-Pb isotopic compositions. It is our expectation that progress in understanding the controls on Pb loss in zircon will come from direct comparison of SAXS and SHRIMP data on the same zircon volumes in this way, because such studies will quantify the relationship between Pb loss and the existence of microstructural Pb migration pathways.

Acknowledgements The Research at Oak Ridge was sponsored in part by the US Department of Energy under Contract No. DE-AC05_00OR22725 with the Oak Ridge National Laboratory, managed by the UT-Battelle. The manuscript benefited from thoughtful and detailed reviews by G. Fraser, Mernagh, J. Lee and L. Nasdala.

Appendix

Sample calculation of scattering length density for zircon

According to Eq. (5), the scattering length density for X-rays is given by:

$$\rho = (N_A d/M) N_e I_e \ , \qquad \text{(A1)}$$

where $N_A = 6.022 \times 10^{23}$ is Avogadro's number, d is density, M is the molar mass, $I_e = (e^2 mc^{-2})$ is the scattering amplitude for a single electron. N_e is the number of electrons in one "supramolecule" of composition corresponding to the average elemental composition of a macroscopic phase of density d present in the scattering medium, whose elemental composition can be expressed as:

$$\Sigma_j p_j (\Sigma_i s_i)_j \ , \qquad \text{(A2)}$$

where s_i is the proportion by number of atom i in the compound j and p_j is the proportion by molecular number of compound j in the macroscopic phase. Formula (A2) is quite general and covers cases as complex as a very fine mix of numerous oxides, specified with the running index j, comprising for instance an inorganic matrix of a mudstone.

For zircons, the elemental composition is $ZrSiO_4$. Zr atom (atomic mass 91.224) has 40 electrons, Si atom (atomic mass 28.0855) has 14 electrons and the O atom (atomic mass 15.9994) has 8 electrons, where all the atomic masses are averages over all the naturally abundant isotopes. Therefore, the molar mass of $ZrSiO_4$ is $91.224 + 28.0855 + 4 \times 15.9994 = 183.3071$ g, and the total number of electrons in one molecule is $40 + 14 + 4 \times 8 = 86$.

The scattering amplitude for a single electron is $I_e = (e^2 mc^{-2})$, where m is the mass of an electron, e its charge and c is the velocity of light in vacuum. Substituting $m = 9.10939 \times 10^{-28}$ g, $e = 1.6022 \times 10^{-19}$ $C = 4.80298 \times 10^{-10}$ $cm^{3/2}$ $g^{1/2}$ s^{-1}, and $c = 299792458$ m s^{-1}, one gets $I_e = 2.8177 \times 10^{-13}$ cm.

The scattering length density, ρ, for crystalline zircon can be now calculated from formula (A1) by substituting $I_e = 2.8177 \times 10^{-13}$ cm, $N_A = 6.022 \times 10^{-23}$, $M = 183.3071$ g, $N_e = 86$ and the density $d = 4.72$ gcm^{-3} (Table 2). The result is $\rho = 3.757 \times 10^{11}$ cm^{-2}. For metamict zircon the only difference is the density, which now is $d = 4.0$ g cm^{-3} (Table 2), and the resulting scattering length density is $\rho = 3.184 \times 10^{11}$ cm^{-2}. Given the uncertainties in the zircon density, the values of the scattering length density presented in Table 2 have been rounded to three significant digits.

References

Chakoumakos BC, Murakami T, Lumpkin GR, Ewing RC (1987) Alpha-decay-induced fracturing in zircon: the transition from the crystalline to the metamict state. Science 236: 1556–1559

Cherniak DJ, Watson EB (2000) Pb diffusion in zircon. Chem Geol 172: 5–24

Cherniak DJ, Lanford WA, Ryerson FJ (1991) Lead diffusion in apatite and zircon using ion implantation and Rutherford backscattering techniques. Geochim Cosmochim Acta 55: 1663–1673

Claoue-Long JC, Compston W, Roberts J, Fanning CM (1995) Two Carboniferous ages: a comparison of SHRIMP zircon dating with conventional zircon ages and $^{40}Ar/^{39}Ar$ analysis. SEPM (Society for Sedimentary Geology) Spec Publ 54: 3–21

Lee JKW, Williams IS, Ellis DJ (1997) Pb, U and Th diffusion in natural zircon. Nature 390: 169–162

Compston W, Williams IS, Meyer C (1984) U–Pb geochronology of zircons from lunar breccia 73217 using a sensitive high mass-resolution ion microprobe. J Geophys Res 89: B525–534

Espinat D (1990) Application des techniques de diffusion de la lumiere des rayons X et des neutrons a l'etude des systemes colloidaux. Rev Inst Franc Petr 45(6): 1–131

Ewing RC, Chakoumakos GR, Lumpkin GR, Murakami T (1987) The metamict state. Mineral Res Bull 12: 58–66

Faure G (1986) Principles of isotope geology. Wiley, New York, 589 pp

Froude DO, Ireland TR, Kinny PD, Williams IS, Compston W (1983) Ion microprobe identification of 4100–4200 Myr-old terrestrial zircons. Nature 304: 616–618

Guinier A, Fournet G, Walker CB, Yudowitch KL (1955) Small-angle scattering of X-rays. John Wiley, New York, 259 pp

Glatter O, Kratky O (1982) Small-angle X-ray scattering. Academic Press, London

Holland HD, Gottfried D (1955) The effect of nuclear radiation on the structure of zircon. Acta Crystallogr 8: 291–300

Lee JKW (1993) Problems and progress in the elucidation of U and Pb transport mechanisms in zircon. In: Boland JN and FitzGerald JD (eds) Defects and processes in the solid state: geoscience applications. The McLaren Volume. Elsevier, Amsterdam, pp 423–446

Lee JKW (1995) Multipath diffusion in geochronology. Contrib Mineral Petrol 120: 60–82

Lee JKW, Tromp J (1995) Self-induced fracture generation in zircon. J Geophys Res 100: (B)17753–17770

Lee JKW, Williams IS, Ellis DJ (1997) Pb, U and Th diffusion in natural zircon. Nature 390: 159–162

Lindner P, Zemb T (eds) (1991) Neutron X-ray and light scattering. Elsevier, Amsterdam

McDougall I, Harrison TM (1999) Geochronology and thermochronology by the $^{40}Ar/^{39}Ar$ method. Oxford University Press, UK, 269 pp

McLaren AC, Fitz Gerald JD, Williams IS (1994) The microstructure of zircon and its influence on the age determination from Pb/U isotopic ratios measured by ion microprobe. Geochim Cosmochim Acta 58(2): 993–1005

Murakami T, Chakoumakos BC, Ewing RC, Lumpkin GR, Weber WJ (1991) Alpha-decay event damage in zircon. Am Mineral 76(9–10): 1510–1532

Nasdala L, Pidgeon RT, Wolf D (1996) Heterogeneous metamictization of zircon on a microscale. Geochim Cosmochim Acta 60: 1091–1097

Nasdala L, Pidgeon RT, Wolf D, Irmer G (1998) Metamictization and U-Pb isotopic discordance in single zircons: a combined Raman microprobe and SHRIMP ion probe study. Mineral Petrol 62: 1–27

Nasdala L, Wenzel M, Vavra G, Irmer G, Wenzel T, Kober B (2001) Metamictization of natural zircon: accumulation versus thermal annealing of radioactivity-induced damage. Contrib Mineral Petrol 141: 125–144.

Nasdala L, Lengauer CL, Hanchar JM, Kronz A, Wirth R, Blanc P, Kennedy AK, Seydoux-Guilleaume A-M (2002) Chem Geol 191/1–3: 121–140

Ozkan H (1976) Effect of nuclear radiation on the elastic moduli of zircon. J Appl Geophys 47: 4772–4779

Pigeon RT, Nemchin AA, Hitchen GJ (1998) Internal structures of zircons from Archean granites from the Darling Range batholith: implications for zircon stability and the interpretation of zircon U–Pb ages. Contrib Mineral Petrol 132: 288–299

Radlinski AP, Boreham CJ, Lindner P, Randl OG, Wignall GD, Hinde AL, Hope HM (2000) Small-angle neutron scattering signature of oil generation in artificially and naturally matured hydrocarbon source rocks. Organ Geochem 31: 1–14

Radlinski AP, Mastalerz M, Hinde AL, Hainbuchner M, Rauch H, Baron M, Lin J-S, Fan L, Thiyagarajan P (2001) Non-invasive measurements of pore size distribution in coal pellets using X-ray and neutron techniques. Proceedings International Coalbed Methane Symposium 2001 May 14–18 Bryant Conference Center, The University of Alabama, Tuscaloosa, Alabama USA 163–175

Radlinski AP, Ioannidis MA, Hinde AL, Hainbuchner M, Baron M, Rauch H, Kline SR (2003) Angstrom to millimeter characterization of sedimentary rock structure. J Colloid Interface Sci (in press)

Riekel C (1998) Micro X-ray small-angle scattering with synchrotron radiation. J Macromol Sci Phys (B)37(4): 587–599

Russell TP, Lin J-S, Spooner S, Wignall GD (1988) Intercallibration of small-angle X-ray and neutron scattering data. J Appl Crystallogr 21: 629–638

Salje EKH, Chrosch J, Ewing RC (1999) Is metamictization of zircon a phase transition? Am Mineral 84: 1107–1116

Weber WJ (1993) Alpha-decay-induced amorphization in complex silicate structures. J Am Ceram Soc 76: 1729–1738

Williams IS (1998) U–Th–Pb geochronology by ion microprobe. Rev Econ Geol 7: 1–35

Yada K, Tanki T, Sunagawa I (1987) Radiation-induced lattice defects in natural zircon ($ZrSiO_4$) observed at atomic resolution. Phys Chem Miner 14: 197–204